MedChemComm

REVIEW

View Article Online
View Journal | View Issue

Check for updates

Cite this: *Med. Chem. Commun.*, 2017, **8**, 1393

Recent progress in the development of metal complexes as β-amyloid imaging probes in the brain

Kaihua Chen and Mengchao Cui *

Received 5th February 2017,
Accepted 11th May 2017

DOI: 10.1039/c7md00064b

rsc.li/medchemcomm

In this review, we have focused on the recent progress in metal complexes that are able to bind to β-amyloid (Aβ) species. We have discussed various radioactive complexes of ^{99m}Tc, ^{68}Ga, ^{64}Cu, ^{89}Zr, and ^{111}In, which were designed as Aβ imaging agents for positron emission tomography (PET) and single photon emission computed tomography (SPECT) imaging, non-radioactive Re and Ru complexes as Aβ sensors using luminescence methods, and Gd^{3+} complexes as contrast agents for magnetic resonance imaging (MRI).

Published on 16 May 2017. Downloaded by RSC Internal on 31/05/2018 13:36:39.

1. Introduction

Alzheimer's disease (AD) is a neurodegenerative brain disease that leads to synaptic reduction and cognitive decline. It is the most common cause of dementia and may eventually lead to death among elderly patients.[1] Cerebral amyloid angiopathy (CAA) is a disorder that has been recognized as an important cause of lobar intracerebral hemorrhage (ICH), microbleeds (MBs), ischemic stroke, and dementia.[2,3] It has been estimated that CAA occurs in up to 80% of patients with AD; approximately 25% of these patients experienced severe CAA.[4–6] According to the amyloid cascade hypothesis, the mismetabolism of the amyloid precursor protein (APP) is the initial event in the pathogenesis of AD, which subsequently leads to the aggregation of the β-amyloid (Aβ) protein, specifically $A\beta_{1-40/42}$.[7,8] Histopathological studies have shown extensive Aβ deposition in the cerebral cortex in the post-mortem analysis of patients with AD, while Aβ deposition was mainly observed in the walls of the leptomeningeal and cortical arterioles of patients with CAA.[9,10] The *in vivo* imaging of the deposition of Aβ plaques in the brain has been accepted as a useful tool in the study of the pathophysiology of neurodegenerative diseases associated with misfolded Aβ species.[11] Therefore, it is of great importance to precisely detect Aβ in the preclinical diagnosis of AD and CAA with the use of non-invasive imaging techniques.[12,13] To achieve this, various imaging modalities, including nuclear imaging techniques, such as positron emission tomography (PET) and single photon emission computed tomography (SPECT), magnetic resonance imaging (MRI), and optical imaging techniques, for example near-infrared (NIR) imaging methods, have been employed.[14,15]

Key Laboratory of Radiopharmaceuticals, Ministry of Education, College of Chemistry, Beijing Normal University, Beijing 100875, P. R. China.
E-mail: cmc@bnu.edu.cn; Fax: +86 10 58808891; Tel: +86 10 58808891

In the past decades, many radiolabeled tracers aimed at the detection of Aβ in live patients with AD have been developed and evaluated. 2-(4-[^{11}C]Methylaminophenyl)-6-hydroxybenzothiazole ([^{11}C]PIB, **1**)[16–18] is the most commonly used imaging agent for PET imaging. [^{18}F]-Flutemetamol ([^{18}F]GE-067, **2**),[19,20] [^{18}F]florbetapir ([^{18}F]AV-45, **3**),[21–23] and [^{18}F]florbetaben ([^{18}F]BAY-94-9172, **4**)[24,25] were successively approved by the FDA (Fig. 1). However, noninvasive methods for the selective and accurate detection and quantification of the Aβ burden of CAA have not yet been established. The study of CAA imaging agents is still in an early stage, with only a few reported so far; examples include the ^{18}F-polypegylated styrylpyridines (**5–7**) reported by Kung *et al.*[26] and the fluorescent resorufin analogs (**8–10**) reported by Han *et al.* (Fig. 1).[27]

Metal complexes, which contain radionuclides, such as ^{99m}Tc, ^{68}Ga, ^{64}Cu, ^{89}Zr, and ^{111}In, can be utilized as PET or SPECT Aβ imaging probes. Non-radioactive metal complexes,

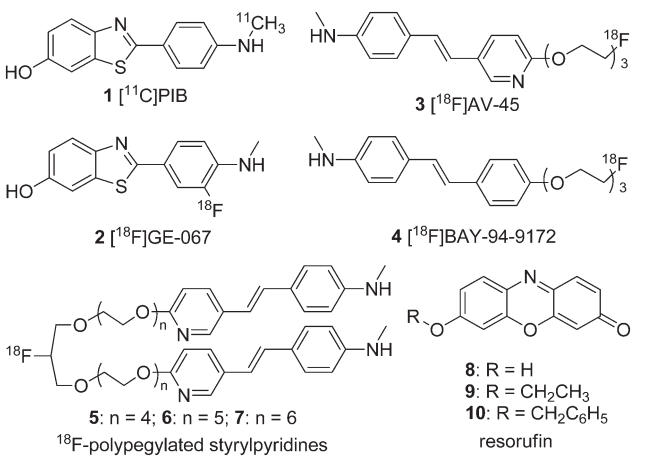

Fig. 1 Chemical structures of Aβ imaging probes designed for AD and CAA.

Published on 16 May 2017. Downloaded by RSC Internal on 31/05/2018 13:36:39.

such as phosphorescent rhenium and ruthenium complexes, which have good photophysical properties, can be used as non-conventional probes in the fluorescence imaging of amyloid formation, while gadolinium complexes can be used as MRI imaging agents for Aβ deposits. In 2014, a detailed review of metal complexes designed to bind to Aβ for the diagnosis and treatment of AD was conducted by Donnelly *et al.*[28] However, in the intervening three years, many meaningful metal complexes have been developed for Aβ detection. Thus, this review will discuss the metal complexes designed and evaluated for the detection of Aβ deposits in AD or CAA that were developed between 2014 and 2017.

2. Radioactive metal complexes as Aβ imaging probes

2.1. ^{99m}Tc-labeled complexes for SPECT imaging

Despite the rapid increase in the number of hospitals equipped with the requisite infrastructure for PET, SPECT is still the most commonly used nuclear imaging technique. Currently, the ^{99m}Tc isotope is the most widely used radionuclide in medical diagnostic procedures using SPECT, owing to its good radioactive characteristics, such as the emission of readily detectable gamma rays (140 keV), an appropriate half-life (6.01 h), and easy production by ^{99m}Tc/^{99}Mo generators. Thus, the development of new ^{99m}Tc-labeled imaging agents will provide simple, convenient, and widespread SPECT-based methods for the detection and quantitative analysis of Aβ plaques. All isotopes of technetium are radioactive. Rhenium is a congener of technetium in group VII and has a similar ionic radius to technetium. Thus, rhenium is always used to form analogs of ^{99m}Tc complexes for comprehensive characterization and preliminary *in vitro* assessments.[29] Many ^{99m}Tc-labeled Aβ imaging agents have been previously reported.[14,30] In the following section, we have described the significant progress towards ^{99m}Tc complexes for Aβ plaque imaging published from 2014 onwards. In order to incorporate the transition metal ^{99m}Tc into a small organic molecule, a chelating structure is essential. Two common cores, $[^{99m}TcO]^{3+}$ and $[^{99m}Tc(CO)_3]^{+}$, are described in this review.

2.1.1. $[^{99m}TcO]^{3+}$ complexes with tetradentate chelators. The $[^{99m}TcO]^{3+}$ core forms square pyramidal oxo-technetium complexes with multiple tetradentate chelators, such as N_2S_2, N_2O_2, N_3S, and N_3O bifunctional chelators (Fig. 2).[31,32]

The tetradentate N_2S_2 chelators, which include bis-aminoethanethiol (BAT) and monoamine-monoamidedithiol (MAMA), can easily form relatively small, stable, and neutral complexes with the $[^{99m}TcO]^{3+}$ core. Based on the conjugate approach, various $[^{99m}TcO]^{3+}$ complexes, such as Congo red, chrysamine G,[33,34] phenylbenzothiazole,[35–37] phenylbenzoxazole,[38] phenylbenzofuran,[39,40] flavone,[41] aurone,[41] chalcone,[42] curcumin,[43] naphthalene,[44] dibenzylideneacetone[45] and stilbene[46] coupled with MAMA and BAT bifunctional chelators have been reported.

Cui *et al.* reported two novel uncharged ^{99m}Tc/Re-labeled 2-phenylbenzoxazole derivatives conjugated with BAT and MAMA chelators *via* a pentyloxy spacer (**11** and **12**, Fig. 3).[38]

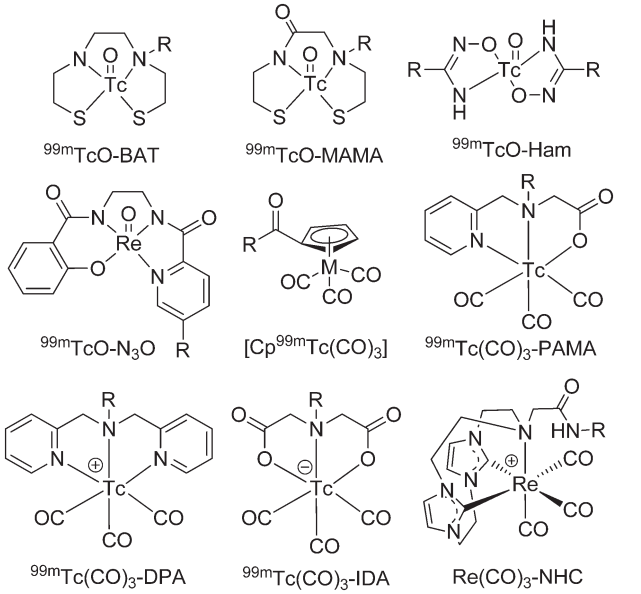

Fig. 2 Chemical structures of bifunctional chelators used for ^{99m}Tc-labeled Aβ imaging probes.

Both compounds displayed a high binding affinity for $A\beta_{1-42}$ (**11** and **12**, K_i = 11.1 and 14.3 nM, respectively). According to the biological evaluation, the TcOBAT complex (**11**, Table 1) has advantages over the TcOMAMA complex (**12**, Table 1) as an Aβ targeting probe, with a higher initial brain uptake (0.81% ID g^{-1} *vs.* 0.43% ID g^{-1} at 2 min) and a faster wash-out rate (0.25% ID g^{-1} *vs.* 0.30% ID g^{-1} at 60 min) from the brain of normal mice. Additionally, four new 2-arylbenzoxazole derivatives conjugated with the BAT

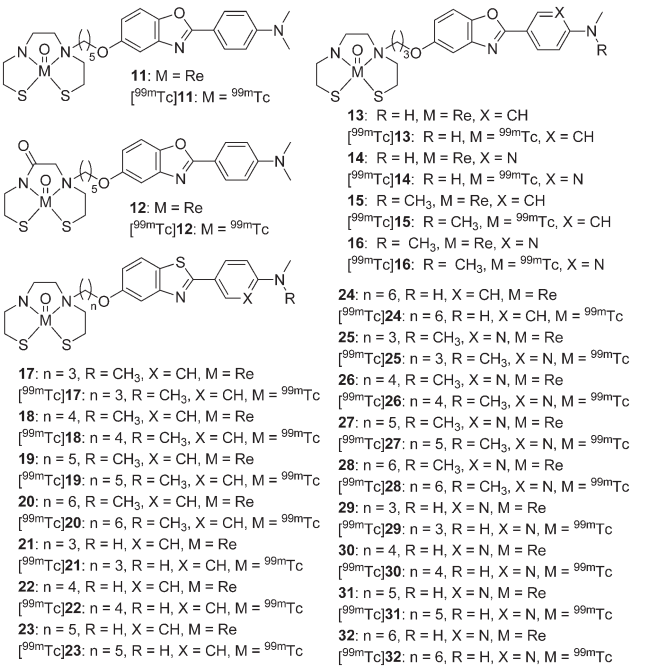

Fig. 3 Chemical structures of ^{99m}Tc/Re-labeled 2-arylbenzoxazoles and 2-arylbenzothiazoles conjugated with BAT and MAMA chelators.

 This journal is © The Royal Society of Chemistry 2017

Published on 16 May 2017. Downloaded by RSC Internal on 31/05/2018 13:36:39.

Table 1 Binding affinities and brain pharmacokinetics of $[^{99m}TcO]^{3+}$ complexes with tetradentate chelators

No.	$A\beta_{1-42}$ K_i (nM)	$A\beta_{1-40}$ K_i (nM)	Brain uptake (% ID g^{-1}) 2 min	60 min	Ref.
11	11.1	—	0.81	0.25	38
12	14.3	—	0.43	0.30	38
13	128.2	—	1.10	0.31	47
14	393.2	—	0.96	0.15	47
15	15.9	—	1.55	0.40	47
16	37.2	—	1.24	0.14	47
17	56.6	—	—	—	48
18	16.0	—	0.69	0.46	48
19	33.5	—	0.46	0.40	48
20	8.4	—	0.59	0.43	48
21	2303.0	—	—	—	48
22	8.8	—	2.11	0.62	48
23	104.9	—	—	—	48
24	29.4	—	0.92	0.63	48
25	105.6	—	—	—	48
26	134.1	—	—	—	48
27	17.6	—	0.47	0.19	48
28	24.4	—	0.60	0.29	48
29	2356.2	—	—	—	48
30	93.6	—	—	—	48
31	440.9	—	—	—	48
32	75.4	—	—	—	48
33A	0.72[a]	0.38[a]	0.37	0.08	52, 53
33B	0.38[a]	0.45[a]	—	—	52, 53
34A	16.40[a]	4.59[a]	0.28	0.11	52, 53
34B	2.55[a]	3.37[a]	—	—	52, 53
35A	0.26[a]	0.24[a]	—	—	52, 53
35B	0.47[a]	0.99[a]	0.36	0.08	52, 53
36A	2.80[a]	1.58[a]	—	—	52, 53
36B	5.78[a]	4.96[a]	0.37	0.05	52, 53
38	0.56	—	0.35	0.11	54
39	855[b]	—	—	—	55

[a] Expressed as IC_{50} values (μM) in the presence of PIB. [b] Measured using fluorescence competition assay against thioflavin-T (ThT).

chelator *via* a short propoxy spacer were reported ([^{99m}Tc]**13–16**, Fig. 3, Table 1).[47] All rhenium analogs (**13–16**) clearly stained Aβ plaques in brain sections from transgenic (Tg) mice and patients with AD. The *in vitro* competition binding assay revealed that the *N*,*N*-dimethylated complexes exhibited a higher affinity to $A\beta_{1-42}$ aggregates (**15** and **16**, K_i = 15.9 and 37.2 nM, respectively) than the *N*-monomethylated complexes (**13** and **14**, K_i = 128.2 and 393.2 nM, respectively). The affinity of the phenyl derivatives (**13** and **15**) was higher than that of the pyridyl analogs (**14** and **16**). In addition, the phenyl derivatives [^{99m}Tc]**13** and [^{99m}Tc]**15** displayed higher initial brain uptake (1.10 and 1.55% ID g^{-1} at 2 min) than the pyridyl derivatives [^{99m}Tc]**14** and [^{99m}Tc]**16** (0.96 and 1.24% ID g^{-1} at 2 min). Among these ^{99m}Tc-labeled 2-arylbenzoxazole derivatives, [^{99m}Tc]**15** displayed higher initial brain uptake (1.55% ID g^{-1} at 2 min), but a comparable $brain_{2min}/brain_{60min}$ ratio (3.38). However, the blood–brain barrier (BBB) penetrability of [^{99m}Tc]**15** is still lower than ideal and requires further modifications. In addition, two stereoisomers were generated when the $[^{99m}TcO]^{3+}$ core coordinated with MAMA or BAT chelators. The X-ray crystallography of the rhenium complex **13** revealed that the *syn* isomer was the major product.

To further improve the brain pharmacokinetics of ^{99m}Tc-labeled probes for Aβ plaques, Cui *et al.* reported the systematic study of a series of 2-arylbenzothiazole derivatives conjugated with the BAT chelator *via* different lengths of alkyl linkers (n = 3–6) (**17–32**, Fig. 3 and Table 1).[48] Different aminomethyl groups and lengths of alkyl linkers were employed to balance the binding affinity and BBB permeability. Seven rhenium complexes with relatively longer alkyl chains (**18–20**, **22**, **24**, **27**, and **28**) exhibited a strong binding affinity toward $A\beta_{1-42}$ aggregates (K_i < 50 nM). These compounds were selected for ^{99m}Tc-labeling and further evaluation. All of the ^{99m}Tc-labeled complexes displayed good affinity and specificity to Aβ plaques in Tg mouse brain tissue in the *in vitro* autoradiography studies. Among them, [^{99m}Tc]**22** showed both a high binding affinity (K_i = 8.8 nM) and favorable brain pharmacokinetics in normal mice (2.11% ID g^{-1} at 2 min and 0.62% ID g^{-1} at 60 min). *Ex vivo* autoradiography revealed that [^{99m}Tc]**22** could penetrate the BBB and intensely label Aβ plaques in the brain of Tg mice. Thereafter, [^{99m}Tc]**22** was selected as the first ^{99m}Tc-labeled Aβ imaging probe for SPECT/CT imaging studies in nonhuman primates. The semiquantitative data and SPECT images revealed that [^{99m}Tc]**22** could penetrate the brain of rhesus monkeys to an average degree of one percent of the injected dose. All these results indicated that [^{99m}Tc]**22** could serve as a potential SPECT imaging probe for Aβ plaques in AD.

However, ligands containing N_2S_2 chelators are air-sensitive and easily oxidized, which makes them difficult to form in a radiopharmaceutical kit. The thiol-free hydroxamamide (Ham) chelator is known to generate ^{99m}Tc-labeled complexes with high stability and high radiochemical yield under mild conditions (room temperature and neutral medium).[49–51] In addition, Ham is a bidentate chelator, which may enhance the binding affinity of the bidentate complexes to Aβ plaques.

Recently, Ono *et al.* designed and synthesized five bidentate ^{99m}Tc–Ham complexes conjugated with the classical Aβ binding motifs of stilbene and 2-phenylbenzothiazole ([^{99m}Tc]**33–36**, Fig. 4 and Table 1) and dimethylaminobenzene ([^{99m}Tc]**37**, Fig. 4).[52] According to the results for the reaction mixture analyzed by radio-HPLC, two radioactive isomers were produced in the ^{99m}Tc complexation reaction with Ham. They defined the shorter retention time isomers as either **A**-form ([^{99m}Tc]**33A**, [^{99m}Tc]**34A**, [^{99m}Tc]**35A**, [^{99m}Tc]**36A**, and [^{99m}Tc]**37A**) or **B**-form ([^{99m}Tc]**33B**, [^{99m}Tc]**34B**, [^{99m}Tc]**35B**, [^{99m}Tc]**36B**, and [^{99m}Tc]**37B**). The *in vitro* inhibition assay indicated that the bivalent ^{99m}Tc–Ham complexes ([^{99m}Tc]**34A**, [^{99m}Tc]**34B**, [^{99m}Tc]**36A**, and [^{99m}Tc]**36B**) displayed much higher binding affinities for amyloid aggregates than the monovalent complexes ([^{99m}Tc]**33A**, [^{99m}Tc]**33B**, [^{99m}Tc]**35A**, and [^{99m}Tc]**35B**). The high binding affinity of these ^{99m}Tc–Ham complexes was further confirmed by *in vitro* autoradiography studies using brain sections from Tg2576 mice. In addition, significant differences between the two isomers were observed in their

Published on 16 May 2017. Downloaded by RSC Internal on 31/05/2018 13:36:39.

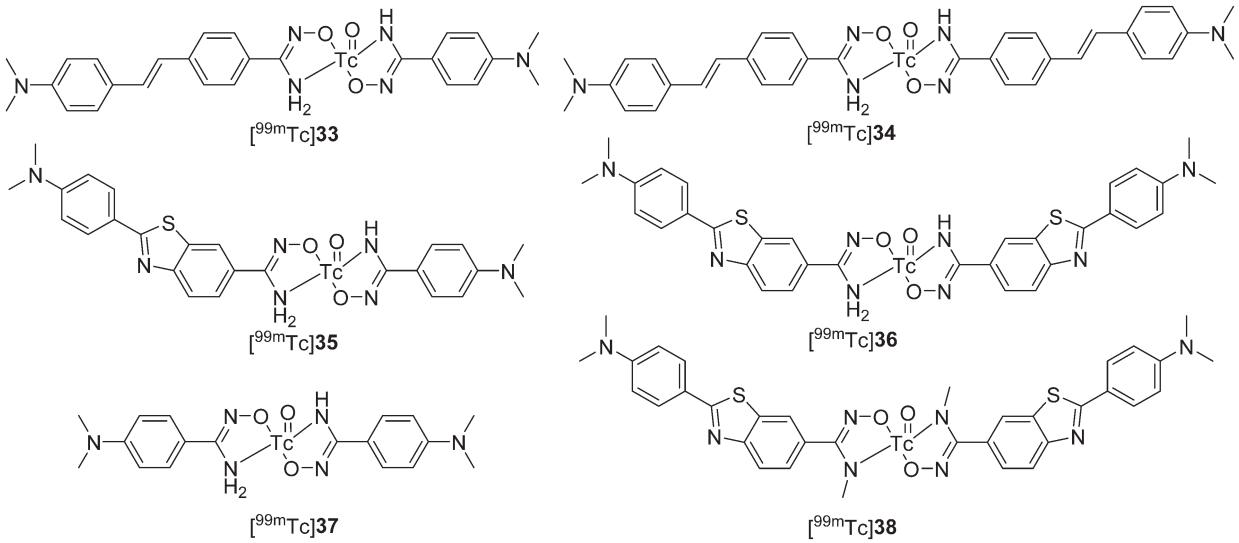

Fig. 4 Chemical structures of ^{99m}Tc–Ham complexes with bivalent amyloid ligands.

binding ability; [^{99m}Tc]**37** with two dimethylaminobenzene substituents did not bind to amyloid aggregates. In biodistribution studies, [^{99m}Tc]**34A**, which had the highest binding affinity, displayed poor brain uptake (0.28% ID g^{-1} at 2 min) in normal mice, which indicated that these ^{99m}Tc–Ham complexes were unable to penetrate the BBB and were thus unsuitable for application to AD diagnosis. However, they may be used as imaging agents for the diagnosis of CAA.

Thereafter, these ^{99m}Tc–Ham complexes were evaluated as CAA-specific imaging probes.[53] Considering that $A\beta_{1-40}$ is more abundant in the cerebrovascular amyloid of CAA, an *in vitro* binding study was performed using $A\beta_{1-40}$ aggregates. Similar to the results using $A\beta_{1-42}$ aggregates, dimer complexes displayed stronger binding than monomer complexes. The high binding ability was further verified by *in vitro* autoradiography studies using human CAA brain sections from two different patients; both [^{99m}Tc]**34A** and [^{99m}Tc]**36B** displayed intensive labeling of Aβ deposits. Finally, the specific binding of [^{99m}Tc]**34A** and [^{99m}Tc]**36B** to the cerebrovascular amyloid was verified by *ex vivo* autoradiography studies using Tg2576 mice; the complexes displayed low brain entry and selective binding to vascular Aβ deposits in the model mice, but not in the wild-type (WT) mice. These results indicated that the bivalent ^{99m}Tc–Ham complexes, [^{99m}Tc]**34A** and [^{99m}Tc]**36B**, could specifically detect CAA *in vivo*. However, two geometric isomers of these ^{99m}Tc–Ham complexes (**A**-form and **B**-form) were observed in the ^{99m}Tc-labeling reaction, which might complicate their clinical application.

To avoid the formation of isomers, an *N*-methyl-substituted Ham chelator conjugated with 2-phenylbenzothiazole was designed and evaluated.[54] A single ^{99m}Tc–Ham complex, [^{99m}Tc]**38**, was obtained with notable stability. Although [^{99m}Tc]**38** displayed lower binding affinity for Aβ aggregates (IC_{50} = 0.56 μM) than the parent ^{99m}Tc–Ham complex ([^{99m}Tc]**38B**, IC_{50} = 5.78 μM), specific labeling of the Aβ deposits was still observed in the *in vitro* autoradiography studies of brain sections from Tg2576 mice and patients with CAA. Similar to other ^{99m}Tc–Ham complexes, [^{99m}Tc]**38** displayed very low brain uptake (0.35% ID g^{-1} at 2 min), which was favorable for CAA-specific imaging.

Donnelly *et al.* designed new non-thiol-based semirigid tetradentate hybrid N_3O chelating agents to form neutral lipophilic complexes with oxotechnetium(v) and oxorhenium(v).[55] Without the thiol group and tertiary amines, two advantages, antioxidation and the preclusion of the formation of *syn* and *anti* diastereomers, were achieved by this N_3O chelator. The ^{99m}Tc/Re complex (**39** and [^{99m}Tc]**39**, Fig. 5, Table 1) with a styrylpyridyl Aβ binding group was prepared. However, the binding affinity of **39** for $A\beta_{1-42}$ fibrils was relatively low (K_i = 855 nM), which was unfavorable as an amyloid imaging agent. However, further biological evaluation, including autoradiography and *in vivo* brain penetration tests, of [^{99m}Tc]**39** was not reported.

2.1.2. [^{99m}Tc(CO)$_3$]$^+$ complexes with various chelators. In recent years, [^{99m}Tc(CO)$_3$]$^+$ has been a popular core for the development of organometallic radiopharmaceuticals.[56] The three water molecules in the [^{99m}Tc(CO)$_3$(H$_2$O)$_3$]$^+$ intermediate

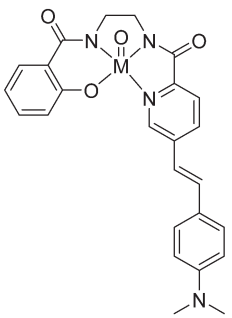

39: M = Re; [^{99m}Tc]**39**: M = ^{99m}Tc

Fig. 5 Chemical structure of ^{99m}Tc/Re-labeled styrylpyridyl conjugated with the N_3O chelator.

 This journal is © The Royal Society of Chemistry 2017

Published on 16 May 2017. Downloaded by RSC Internal on 31/05/2018 13:36:39.

could be easily replaced by tridentate and cyclopentadiene chelators to generate charged or neutral complexes with high yield and stability.[57,58]

Tridentate chelators, containing pyridines, amines, and carboxylate donors conjugated to $[M(CO)_3]^+$, have rapid kinetics and good stability in aqueous solution, which allow the convenience of a kit formulation. The most commonly used tridentate chelators are picolylamine monoacetic acid (PAMA), bis(pyridin-2-ylmethyl)amine (DPA), and iminodiacetic acid (IDA), which generate $^{99m}Tc/Re(CO)_3$ complexes with neutral, positive, and negative charges, respectively (Fig. 2).[59]

Satpati *et al.* reported a neutral 2-phenylbenzothiazole-based $^{99m}Tc(CO)_3$ complex ([^{99m}Tc]**40**, Fig. 6) using the tridentate chelator PAMA with high radiochemical yield (95%). The total binding of [^{99m}Tc]**40** to $A\beta_{1-42}$ aggregates was calculated to be 4.6 ± 0.3%, and the binding was inhibited (26.7 ± 0.6%) by the addition of excessive ThT. In the *in vivo* studies, [^{99m}Tc]**40** displayed low brain uptake (0.25 ± 0.04% ID g^{-1} at 2 min, Table 2), which was unfavorable as an imaging agent for the diagnosis of AD.[60]

Donnelly *et al.* synthesized two pyridylamine-carboxylate tridentate ligands and two dipyridylamine ligands conjugated with stilbene-like Aβ binding motifs *via* a short alkyl linker.[61] In the ^{99m}Tc-labeling reaction, the carboxylate-containing ligands displayed a higher radiochemical yield (>98%) than the dipyridylamine ligands (40–50%). The binding affinity of the rhenium complexes to the Aβ plaques was measured by fluorescence staining in human brain tissue. Complexes **41** and **43** resulted in almost no staining of the Aβ plaques in brain tissues from patients with AD, whereas complexes **42** and **44**, with a dimethylamino group, were more promising. The neutral complex [^{99m}Tc]**42** was much more stable than the cationic complex [^{99m}Tc]**44**, and remained stable in human serum at 37 °C for over 3 h. Therefore, [^{99m}Tc]**42** was selected for further evaluation; the *in vivo* biodistribution studies in Tg mice and WT mice indicated that [^{99m}Tc]**42** hardly crossed the BBB (0.25% ID g^{-1} for WT and 0.24% ID g^{-1} for Tg at 2 min post-injection) and no statistically significant difference between WT and Tg mice was observed at either 2 min or 30 min post-injection. The micro-SPECT studies of [^{99m}Tc]**42** in Tg mice further confirmed its low brain uptake.

As described above, probes with high affinity to amyloid plaques and low BBB penetration can be used as CAA-specific imaging agents. The decreased brain uptake may help to distinguish Aβ deposits between the cerebral vessels and brain parenchyma. For decreased brain uptake, the charged $^{99m}Tc/Re(CO)_3$ complexes with the tridentate chelators, DPA and IDA, are a good choice.

Cui *et al.* reported the synthesis and characterization of four ^{99m}Tc/Re-labeled 2-phenylbenzothiazole and stilbene complexes with a relatively large DPA chelator through a conjugate approach (Fig. 6).[62] The positively charged complexes were considered to have poor BBB penetrability and could specifically target Aβ plaques located on the cerebral vessel walls. Complexes with a five-carbon linker exhibited higher binding

Table 2 Binding affinities and brain pharmacokinetics of $[CpM(CO)_3]$ complexes

No.	$A\beta_{1-42}$ K_i (nM)	Brain uptake (% ID g^{-1}) 2 min	60 min	Ref.
40	—	0.25	0.11	60
42	—	0.25[a]	0.21[a,c]	61
	—	0.24[b]	0.19[b,c]	61
45	162	—	—	62
46	37	0.18	0.08	62
47	366	—	—	62
48	78	0.24	0.10	62
49	106.0	—	—	63
50	45.3	0.80	0.69	63
51	46.0	—	—	63
52	61.9	0.61	0.24	63
53	85.1	—	—	63
54	50.8	0.88	0.15	63
55	56.6	—	—	63
56	42.2, 37.0,[d] 64.5[e]	1.21	0.06	63
57	142.6	0.50	0.18	64
58	75.8	0.36	0.19	64
59	64.1	0.26	0.11	64
60	24.0	0.37	0.14	64
61	18.8	1.06	0.39	65
62	22.8	—	—	65
63	12.4	0.70	0.17	65
64	22.3	—	—	65
65	204.1	—	—	65
66	42.0	0.69	0.31	65
67	130.6	—	—	65
68	15.1	0.54	0.10	65

[a] The brain uptake was measured in WT mice. [b] The brain uptake was measured in 10 month-old APP/PS1 Tg mice. [c] Expressed as brain uptake determined at 30 min post-injection. [d] Expressed as IC_{50} values (nM) for $A\beta_{1-40}$ aggregates. [e] Expressed as IC_{50} values (nM).

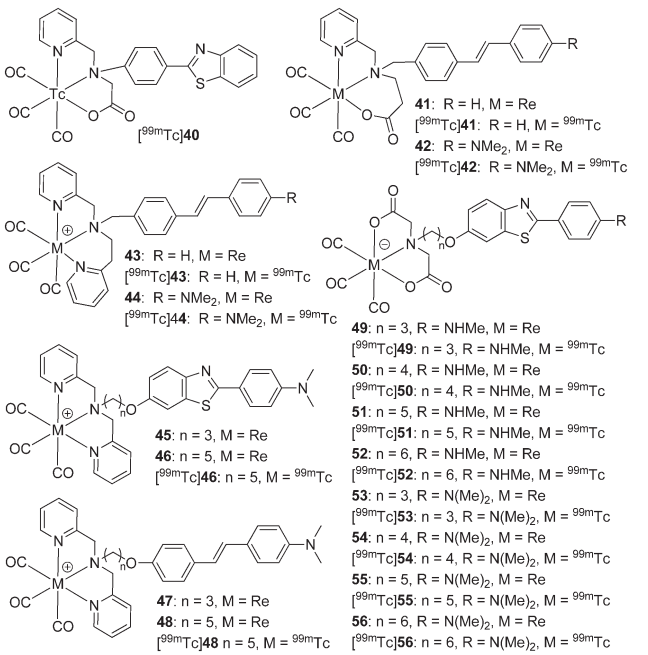

Fig. 6 Chemical structures of $[M(CO)_3]^+$ (M = ^{99m}Tc or Re) complexes with tridentate chelators.

Published on 16 May 2017. Downloaded by RSC Internal on 31/05/2018 13:36:39.

affinities (**46** and **48**, K_i = 37 and 78 nM, respectively, Table 2) than those with a three-carbon linker (**45** and **47**, K_i = 162 and 366 nM, respectively, Table 2), which suggested that the appropriate length of the carbon linker reduced the steric hindrance imposed by the bulky metal chelate core on the binding motifs. Under fluorescence staining, the rhenium complexes **46** and **48** intensely labeled the Aβ plaques associated with the blood vessels as well as in the parenchyma of brain tissue from patients with AD. As expected, reduced brain uptake was observed for [^{99m}Tc]**46** and [^{99m}Tc]**48** (0.18 and 0.24% ID g^{-1} at 2 min, respectively). However, further *in vitro* and *ex vivo* autoradiography studies were not reported.

Then, the same group developed a series of 2-phenylbenzothiazole derivatives conjugated with the chelator IDA *via* alkyl linkers with different lengths (n = 3–6) as negatively charged probes to detect cerebrovascular Aβ deposition.[63] The rhenium surrogates **49–56** strongly stained Aβ deposits in Tg mice and AD patients, and also displayed high affinities to Aβ aggregates (K_i = 42.2–106.0 nM, Table 2). In particular, **56**, with the longest carbon linker (n = 6), displayed the highest affinity toward $A\beta_{1-42}$ aggregates (K_i = 42.2 nM). In addition, slightly higher binding affinities of **56** and [^{99m}Tc]**56** toward aggregates of $A\beta_{1-40}$ than those toward $A\beta_{1-42}$ were observed in both the inhibition assay (37.0 nM *vs.* 64.5 nM) and the direct binding assay (10.15% *vs.* 6.48%). *In vitro* autoradiography of brain sections from Tg mice, patients with AD, and patients with CAA confirmed that [^{99m}Tc]**56** possessed sufficient affinity for Aβ plaques. More interestingly, [^{99m}Tc]**56** selectively labeled Aβ deposits in blood vessels, but not Aβ plaques in the parenchyma of brain tissue from AD patients, which is highly favorable for CAA-specific imaging (Fig. 7). This was the first report of a ^{99m}Tc-labeled tracer that displayed positive autoradiography results and selectively detected Aβ within the blood vessels in brain sections of patients with AD. In the biodistribution studies, the $^{99m}Tc(CO)_3$ complexes displayed relatively low initial brain uptake (0.61–1.21% ID g^{-1} at 2 min post-injection). The *ex vivo* autoradiography studies in Tg and WT mice further confirmed the potential of [^{99m}Tc]**56** to selectively recognize Aβ deposits located in cerebral arterioles.

Cyclopentadienyl tricarbonyl complexes ([$CpM(CO)_3$], M = Re, ^{99m}Tc) possess many attractive properties such as small size, low molecular weight, moderate lipophilicity, and high stability,[58,66] which are highly favorable for BBB penetration and may be applied as Aβ imaging agents for the diagnosis of AD. Cui *et al.* synthesized and evaluated a series of 2-arylbenzothiazole derivatives conjugated with [$CpM(CO)_3$] (M = ^{99m}Tc, Re) *via* amide and ester linkers that contained carbon chains with different lengths (n = 3, 5) (Fig. 8, Table 2).[64,65]

The rhenium complexes **57–68** displayed moderate to high affinity for $A\beta_{1-42}$ aggregates (K_i = 12.4–204.1 nM); in general, the tertiary *N*,*N*-dimethylamino substituents and relatively longer carbon linkers were beneficial for the retention of high Aβ affinity. In the *in vitro* fluorescence staining studies, these rhenium complexes displayed intense staining of Aβ deposits in both the cerebral cortex and the cortical vascula-

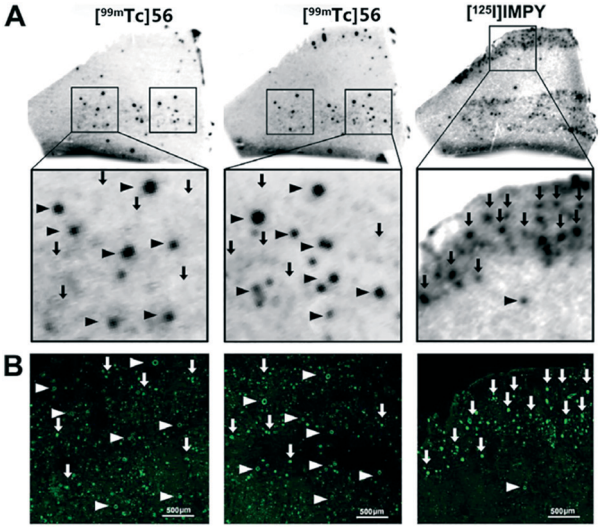

Fig. 7 (A) *In vitro* autoradiography of [^{99m}Tc]**56** and [^{125}I]IMPY on contiguous brain sections of a patient with AD. Aβ deposits within the blood vessels were indicated by triangles and Aβ plaques in the cerebral parenchyma were indicated by arrows. (B) Fluorescence staining using thioflavin-S (ThS) on the same brain sections. Adapted from ref. 63.

ture of brain sections from Tg mice and patients with AD or CAA. Moreover, neurofibrillary tangles were also stained by these rhenium complexes. In the biodistribution studies, all the ^{99m}Tc complexes displayed poor initial brain uptake (0.26–1.06% ID g^{-1}), which impeded their application as Aβ imaging agents for the diagnosis of AD. However, some of them were selected and evaluated as CAA imaging agents. In the *in vitro* autoradiography studies on brain sections from AD patients, [^{99m}Tc]**68** selectively bound to the cerebrovascular Aβ deposits, but not the Aβ plaques, in the parenchyma, which is highly favorable for CAA imaging agents (Fig. 9).

To broaden the scope of potential $^{99m}Tc(CO)_3$-based diagnostic imaging agents for AD, Barnard *et al.* synthesized a

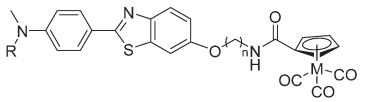

57: n = 3, R = H, M = Re; [^{99m}Tc]**57**: n = 3, R = H, M = ^{99m}Tc
58: n = 5, R = H, M = Re; [^{99m}Tc]**58**: n = 3, R = H, M = ^{99m}Tc
59: n = 3, R = CH_3, M = Re; [^{99m}Tc]**59**: n = 3, R = CH_3, M = ^{99m}Tc
60: n = 5, R = CH_3, M = Re; [^{99m}Tc]**60**: n = 3, R = CH_3, M = ^{99m}Tc

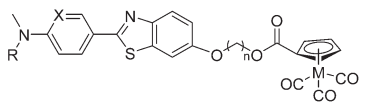

61: n = 3, R = H, X = CH, M = Re; [^{99m}Tc]**61**: n = 3, R = H, X = CH, M = ^{99m}Tc
62: n = 5, R = H, X = CH, M = Re; [^{99m}Tc]**62**: n = 5, R = H, X = CH, M = ^{99m}Tc
63: n = 3, R = CH_3, X = CH, M = Re; [^{99m}Tc]**63**: n = 3, R = CH_3, X = CH, M = ^{99m}Tc
64: n = 5, R = CH_3, X = CH, M = Re; [^{99m}Tc]**64**: n = 5, R = CH_3, X = CH, M = ^{99m}Tc
65: n = 3, R = H, X = N, M = Re; [^{99m}Tc]**65**: n = 3, R = H, X = N, M = ^{99m}Tc
66: n = 5, R = H, X = N, M = Re; [^{99m}Tc]**66**: n = 5, R = H, X = N, M = ^{99m}Tc
67: n = 3, R = CH_3, X = N, M = Re; [^{99m}Tc]**67**: n = 3, R = CH_3, X = N, M = ^{99m}Tc
68: n = 5, R = CH_3, X = N, M = Re; [^{99m}Tc]**68**: n = 5, R = CH_3, X = N, M = ^{99m}Tc

Fig. 8 Chemical structures of 2-arylbenzothiazole derivatives conjugated with the [$CpM(CO)_3$] core.

 This journal is © The Royal Society of Chemistry 2017

Published on 16 May 2017. Downloaded by RSC Internal on 31/05/2018 13:36:39.

series of Re^+ tricarbonyl analogs of novel acyclic and macrocyclic tridentate NHC (N-heterocyclic carbene) ligands coupled to stilbene- or benzothiazole-based amyloid binding groups (Fig. 10).[67] Two linkage isomers will be formed when the acyclic ligands are used (**69a**, **b** and **70a**, **b**), while the macrocyclic ligands produce single complexes (**71** and **72**). The ThT fluorescence assay of **69a**, **70a**, **71**, and **72** to synthetic $A\beta_{1-42}$ fibrils indicated that the they could bind competitively with ThT to $A\beta_{1-42}$ fibrils or that they inhibited the formation of $A\beta_{1-42}$ fibrils. Then, the binding capacity to Aβ plaques of complexes **70a** and **71** was evaluated in human AD brain tissues. Although complex **70a** showed no binding to Aβ plaques, complex **71** displayed co-localization with immunostaining, with a low background. In addition, complex **71** did not show non-specific binding to age-matched controls, according to the epifluorescence images. Thus, the NHC ligands offer possibilities for medicinal inorganic and radiopharmaceutical applications.

2.2. ^{68}Ga-labeled complexes for PET imaging

Among the metal-based radionuclides for PET, gallium-68 ($t_{1/2}$ = 1.13 h, β^+ = 89%) is a prospective radioisotope for PET imaging. The commercial availability of ^{68}Ga from a ^{68}Ge/^{68}Ga generator without an on-site cyclotron permits simple and easy preparation. Moreover, the radiolabeling procedure for ^{68}Ga is quick and simple, requiring a single vial kit solution, and the coordination properties and features of the trivalent gallium are well known and can be easily applied to the development of radiotracers. Although ^{99m}Tc is the most widely used metal-based radionuclide for SPECT imaging, in recent years, attention has been increasingly focused on innovative biomolecules labeled with ^{68}Ga for PET imaging.[68,69]

The most commonly designed chelator for $^{68}Ga^{3+}$ is hexadentate, which is favorable for bifunctional conjugation

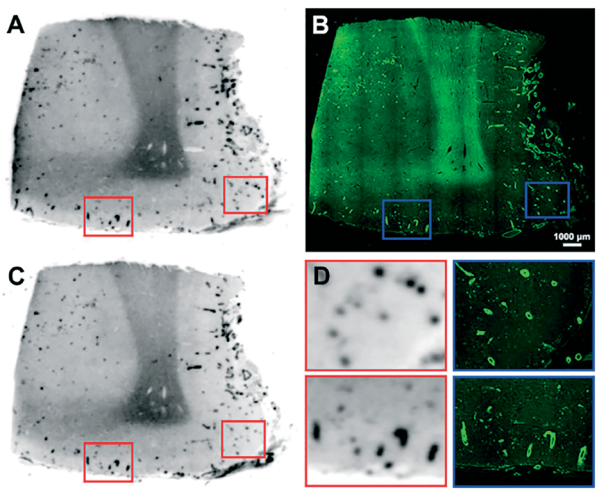

Fig. 9 *In vitro* autoradiography of [^{99m}Tc]**68** binding in contiguous brain sections from a patient with AD (68 years old, female, frontal lobe) (A and C) and the same section stained with ThS (GFP filter) (B). Higher magnification images of A and the corresponding higher magnification images stained with ThS (D). Adapted from ref. 64.

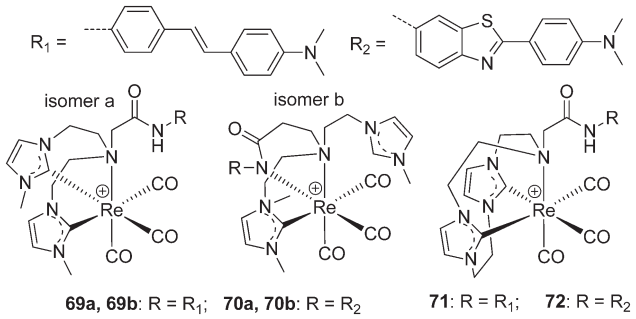

Fig. 10 Chemical structures of $Re(CO)_3$–NHC complexes.

through covalent linkage. When considering the thermodynamic stability of the $^{68}Ga^{3+}$ complex, the best candidates are linear or macrocyclic polyamines modified with negatively charged pendant arms, such as 1,4,7,10-tetraazacyclododecane-1,4,7,10-tetraacetic acid (DOTA), 1,4,7-triazacyclononane-1,4,7-triacetic acid (NOTA), diethylenetriaminepentaacetic acid (DTPA), and *N*,*N*′-bis[2-hydroxy-5-(carboxyethyl)benzyl]ethylenediamine-*N*,*N*′-diacetic acid (HBED) (Fig. 11).[70]

In an attempt to develop efficient and fully automated radiosynthesis of ^{68}Ga-labeled probes for Aβ plaques, Cressier *et al.* reported three uncharged $^{68}Ga^{3+}$-labeled complexes ([^{68}Ga]**73**, [^{68}Ga]**74**, and [^{68}Ga]**75**, Fig. 12) differing in the length of the spacer between the metal-complexing DOTA macrocycle and the peptide-recognizing PIB moiety.[71] However, according to the biological data, these $^{68}Ga^{3+}$-labeled complexes were not potential Aβ imaging probes, as they showed poor brain uptake ([^{68}Ga]**73** or [^{68}Ga]**74**, 0.9–1.1% ID cc^{-1} at 2 min in both animal models; [^{68}Ga]**75**, ~1.3% ID cc^{-1} at 2 min in Tg mice, ~0.5% ID cc^{-1} at 2 min in control mice) and low binding affinity (**73** and **75**, K_d = 170 and 67 μM, respectively) for Aβ deposits. In addition, these complexes failed to detect amyloid deposits through an autoradiographic approach with human brain tissues. Future investigations are needed to enhance the binding affinity and brain uptake of these ^{68}Ga radiotracers.

Ono *et al.* reported a ^{68}Ga-labeled 2-phenylbenzofuran complex conjugated with the DOTA chelator *via* a propoxy linker as

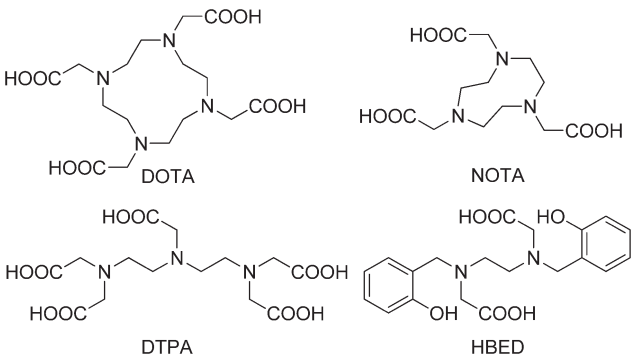

Fig. 11 Chemical structures of commonly designed chelators for $^{68}Ga^{3+}$.

Published on 16 May 2017. Downloaded by RSC Internal on 31/05/2018 13:36:39.

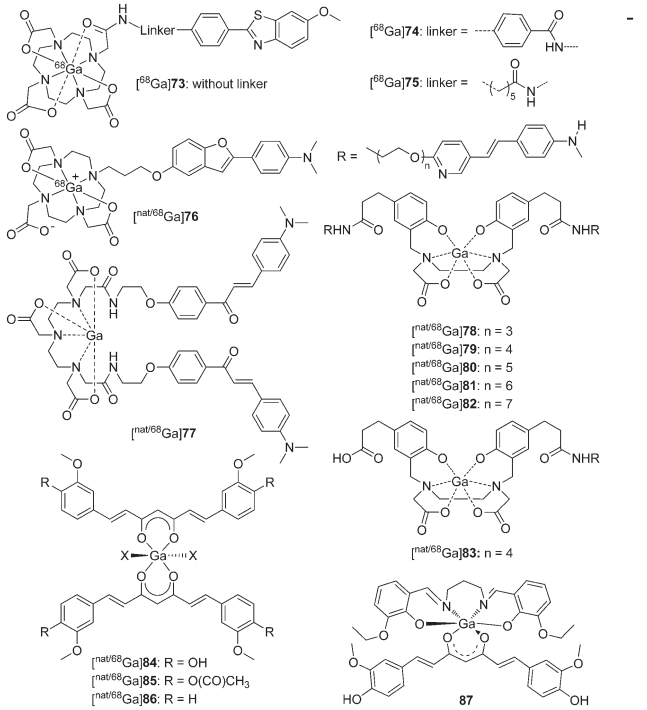

Fig. 12 Chemical structures of $^{nat/68}$Ga-labeled Aβ imaging agents.

an Aβ imaging probe ([$^{nat/68}$Ga]**76**, Fig. 12 and Table 3).[72] The complex [^{nat}Ga]**76** displayed high affinity for $A\beta_{1-42}$ aggregates (K_i = 10.8 nM), which was comparable with other ^{99m}Tc/Re-labeled 2-arylbenzofuran complexes. As expected, clear staining of Aβ plaques was observed in brain sections from Tg2576 mice. However, [^{68}Ga]**76** showed poor initial brain uptake (0.45% ID g^{-1} at 2 min) in biodistribution experiments in normal mice, which may result from the low lipophilicity ($\log P$ = −0.38) and high molecular weight (MW = 706). Therefore, further improvement of the brain uptake appears to be essential for these DOTA-based ^{68}Ga complexes.

Because of the short half-life of ^{68}Ga and the demand for protein and biomolecule labeling, rapid complexation kinetics and mild conditions are favored. However, ^{68}Ga complexation using the DOTA chelator requires a longer reaction time and a temperature of 100 °C, and usually results in lower radiochemical yields. To address these shortcomings, other chelators including DTPA and HBED were introduced for highly efficient radiolabeling with ^{68}Ga at room temperature.[73,74]

An example using a DTPA chelator was reported by Mishra *et al.*, which is the first time that ^{68}Ga complexes have been proposed as Aβ imaging probes ([^{68}Ga]**77**, Fig. 12 and Table 3).[75] The chalcone moiety was selected as the Aβ binding motif, and a homodimeric ligand was designed from the conjugation of two chalcone units with DTPA *via* amide linkage. [^{68}Ga]**77** was obtained under mild conditions with 85.4% efficiency and 9.5–10 MBq nmol^{-1} specific activity. In the *in vitro* binding studies, [$^{nat/68}$Ga]**77** displayed a high binding affinity for $A\beta_{1-42}$ aggregates (K_d = 3.46 nM and K_i = 4.18 nM), which was comparable to the iodinated chalcone derivative. Owing to the incorporation of two chalcone units, the

Table 3 Binding affinities and brain pharmacokinetics of ^{68}Ga, ^{64}Cu, and ^{89}Zr labeled small molecules and mAbs

No.	$A\beta_{1-42}$ K_i (nM)	Brain uptake (% ID g^{-1}) 2 min	60 min	Ref.
73	170[a]	0.9–1.1[b–d]	—	71
74	—	0.9–1.1[b–d]	—	71
75	67[a]	0.5,[b,c] 1.3[b,d]	—	71
76	10.8	0.45	0.27	72
77	4.2, 3.5[e]	1.24	0.20	75
78	30.6[f]	0.12	0.08	76
79	13.4[f]	0.17	0.04	76
80	18.1[f]	0.31	0.11	76
81	6.7[f]	0.21	0.11	76
82	10.7[f]	0.22	0.07	76
83	185[f]	0.11	0.03	76
88	33.7	0.33	0.18	81
89	243.5	0.36	0.21	81
90	0.85[g]	—	0.50	82

[a] Expressed as the K_d value (μM) for $A\beta_{1-40}$ aggregates. [b] Expressed as % ID cc^{-1}. [c] The brain uptake was measured in control mice. [d] The brain uptake was measured in 18 month-old APP/PS1 Tg mice. [e] Expressed as the K_d value (nM). [f] Determined using human AD brain homogenates. [g] Expressed as the K_d value (nM) for $A\beta_{1-40}$ aggregates.

$\log P$ value determined for [^{68}Ga]**77** was 1.58, which was in the optimal range for BBB penetration. Moderate initial brain uptake (1.24% ID g^{-1} at 2 min) and rapid wash-out (0.20% ID g^{-1} at 60 min) were observed for [^{68}Ga]**77** in the *in vivo* biodistribution experiments, which were further validated by dynamic PET studies in normal mice. Similar to ^{99m}Tc-labeled Aβ imaging probes for the diagnosis of AD, the brain uptakes of these ^{68}Ga complexes were still unsatisfactory.

Considering that the ^{68}Ga complexes hardly penetrated the BBB, but may bind to Aβ aggregates on the blood vessel walls, recently, Kung *et al.* reported a series of novel ^{68}Ga complexes with bivalent polypegylated styrylpyridine conjugated to HBED for the detection of CAA with PET.[76] The complexes, [^{68}Ga]**78–83** (Fig. 12), were obtained with high radiochemical yields (93–98%) at room temperature and were stable in both PBS and human plasma. Compared with the monovalent complex ([$^{nat/68}$Ga]**83**, K_i = 185 nM), the bivalent complexes, [$^{nat/68}$Ga]**78–82**, showed improved binding affinity to Aβ plaques in post-mortem AD brain homogenates (K_i = 6.7–30.6 nM, Table 3). *In vitro* autoradiography of post-mortem AD brain sections confirmed their high and specific binding of Aβ plaques. In accordance with other radiometal-labeled complexes, [^{68}Ga]**78–83** showed very low initial brain uptakes (<0.31% ID g^{-1}), which was favorable for CAA-specific imaging. The preliminary results indicated that [^{68}Ga]**78–83** displayed potential to map Aβ plaques in the blood vessels of CAA patients. However, neither *in vitro* autoradiography of these ^{68}Ga complexes using post-mortem CAA brain sections nor *ex vivo* autoradiography using Tg mice was reported and thus the specific and selective binding to CAA was not fully confirmed.

In recent years, radiolabeled curcumin and curcuminoids were reported to have high affinity to Aβ plaques and their potential in the detection of AD was investigated.[77–79] In

 This journal is © The Royal Society of Chemistry 2017

Published on 16 May 2017. Downloaded by RSC Internal on 31/05/2018 13:36:39.

addition, the α,β-diketone group in the middle of the structure allows curcumin to act as an OO bidentate ligand.[43] Asti *et al.* reported three ^{68}Ga-labeled curcumin derivatives ([$^{nat/68}$Ga]**84–86**, Fig. 12) with a 1 : 2 metal-to-ligand molar ratio.[80] All the compounds were obtained with high radiochemical yield (>95%) and showed high stability in both 0.9% NaCl solution and human serum. In preliminary binding studies, these ^{68}Ga complexes displayed moderate-to-high affinity to $A\beta_{1-40}$ aggregates and the specific binding could be inhibited by the addition of excess amounts of the corresponding curcuminoids. Although these preliminary results appear encouraging, further evaluation, including quantitative binding studies and *in vivo* kinetic studies of these ^{68}Ga complexes, is needed to derive the final conclusions.

More recently, Donnelly *et al.* reported a new six-coordinate Ga^{3+} complex (**87**, Fig. 12) by the use of an ancillary tetradentate N_2O_2 Schiff base ligand and the β-diketone group of curcumin as a bidentate ligand.[83] Complex **87** was found to have binding affinity for Aβ plaques in the human brain tissue of patients with AD. However, more efforts, including biological evaluation and radiolabeling, are needed for the validation of this Ga complex as an Aβ imaging agent.

2.3. ^{64}Cu-labeled complexes for PET imaging

The positron-emitting copper-64 radionuclide ($t_{1/2}$ = 12.7 h, β^+ = 17.8%; β^- = 38.4%) has been used in a wide range of applications in targeted radiotherapy and PET imaging.[84] The half-life of ^{64}Cu is long enough for the radiolabeling of small molecules, antibodies, proteins, and nanoparticles. In addition, its low energy positron emission, without much disruptive gamma emission, enables the output of high quality images in comparison with ^{18}F.[85] Owing to the electronic structure of Cu^{2+}, square-planar four-coordinate, square-pyramidal or trigonal-bipyramidal five-coordinate, or octahedral six-coordinate copper complexes could be formed using various chelators with uncharged nitrogen donors and anionic oxygen or sulfur donors. A small number of ^{64}Cu-labeled Aβ imaging probes were reported before 2014 and have been well summarized in a review paper.[28,30]

In 2016, Ono *et al.* reported two novel ^{64}Cu-labeled 2-phenylbenzofuran derivatives conjugated with cyclen ([^{64}Cu]**88**) and DOTA ([^{64}Cu]**89**) as PET imaging probes for Aβ aggregates (Fig. 13 and Table 3).[81] [^{64}Cu]**88** and [^{64}Cu]**89** were obtained with moderate radiochemical yields (72% and 35%) in buffer solution at 85 °C for 10 min. Compared with **88** (K_i = 33.7 nM), complex **89** (K_i = 243.5 nM), with the bulkier chelator DOTA, displayed decreased affinity to Aβ aggregates, which was consistent with the results of *in vitro* fluorescence staining using brain sections from Tg2576 mice, in which **88** showed better results than **89**. Because of the poor brain uptake of [^{64}Cu]**88** and [^{64}Cu]**89** (0.33 and 0.36% ID g^{-1}, respectively) in normal mice, their use as cerebral Aβ imaging probes is inadvisable. However, considering their high affinity and low brain uptake, they may be applicable to CAA or amylin imaging.

2.4. ^{89}Zr-labeled antibodies for PET imaging

Until now, the development of radiolabeled small molecules for the imaging of Aβ plaques has achieved great success. However, as they were all designed to bind to the β-sheet structure of Aβ fibers, the ability and specificity to detect multiple conformations of Aβ are limited.[86] Immuno-PET, with radiolabeled anti-Aβ antibodies, has provided an alternative approach to overcome this issue. Anti-Aβ antibodies, which can detect various Aβ conformations, are able to provide a detailed readout of the amyloid isoform profile in individual subjects.[87–89] Owing to the long biological half-life of monoclonal antibodies (mAbs), which have typical circulation times of 1–3 weeks, the radioisotopes for mAb labeling should also have a similar half-life. Indeed, several Aβ antibodies have been already labeled by radionuclides with a long half-life, such as ^{125}I, ^{124}I, and ^{64}Cu.[89–91] Over the past decade, zirconium-89 has been one of the most popular PET radionuclides for the labeling of mAbs and has the following advantages: appropriate half-life ($t_{1/2}$ = 78.4 h) that is compatible with the circulation time of mAbs; relatively low energy positrons (average energy = 389 keV) for high resolution PET imaging and accurate quantification; the ease of production by means of small medical cyclotrons.[92,93] For metal radionuclides, an appropriate chelator system must be introduced; desferrioxamine B (DFO) is the most commonly used chelator for ^{89}Zr complexation and it is conjugated to the biomolecule before the radiolabeling reaction takes place.[94–96]

More recently, Fissers *et al.* reported a ^{89}Zr-labeled mAb ([^{89}Zr]**90**, [^{89}Zr]Df-Bz-JRF/AβN/25, Fig. 14 and Table 3) for the immuno-PET imaging of Aβ pathology in AD.[82] The bifunctional chelator *p*-isothiocyanatobenzyl-desferrioxamine (Df-Bz-NCS) was coupled to the amino residue of JRF/AβN/25, which is an N-terminal end-specific mAb directed against the full-length human Aβ epitope. The saturation binding assay revealed high and specific binding of [^{89}Zr]**90** to $A\beta_{1-40}$ (K_d = 0.85 nM), which was further validated by *in vitro* autoradiography studies on brain sections from Tg mice (Fig. 15). In the biodistribution studies, [^{89}Zr]**90** demonstrated low brain uptake (0.5 ± 0.07% ID g^{-1} at 1 h) and slow clearance (0.36 ± 0.06% ID g^{-1} at 48 h).

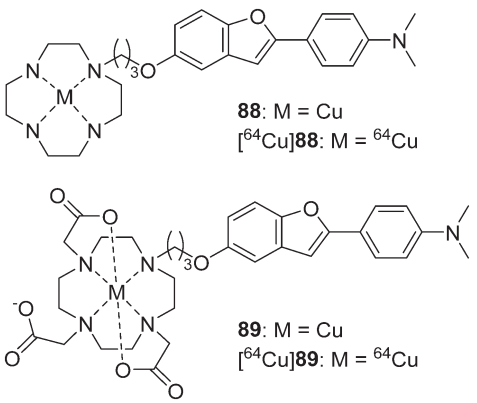

Fig. 13 Chemical structures of ^{64}Cu-labeled 2-phenylbenzofuran derivatives conjugated with cyclen and DOTA.

Published on 16 May 2017. Downloaded by RSC Internal on 31/05/2018 13:36:39.

Therefore, further imaging studies in Tg mice should be performed to evaluate if the *in vivo* brain accumulation of [^{89}Zr]**90** was sufficient to allow accurate Aβ quantification.

2.5. ^{111}In-labeled antibody and Aβ peptide for SPECT imaging

Similar to zirconium-89, indium-111 has a half-life ($t_{1/2}$ = 67.3 h) that is compatible with the circulation time of mAbs; however, indium-111 decays *via* the emission of 171 and 245 keV gamma rays. Thus, ^{111}In has been widely used as a SPECT radioisotope for mAbs labeling.[97]

Van der Weerd *et al.* reported an ^{111}In-labeled fusion protein containing VHH (a llama single-domain antibody fragment used for targeting amyloid plaques in AD).[98] With the aim of increasing the serum persistence, the Fc portion of the human IgG1 antibody (hinge plus CH_2 and CH_3 domains) was fused to the C-terminus of VHH to form VHH–Fc. Then, ^{111}In was introduced by the conjugation of the bifunctional chelator *p*-SCN-Bz-DTPA to the primary amine groups on the VHH–Fc fusion protein ([^{111}In]**91**, [^{111}In]VHH–Fc–DTPA, Fig. 14). Immunofluorescence analysis confirmed that VHH–Fc–DTPA retained its affinity for Aβ deposits in brain sections from patients with AD. Despite the increased blood circulation time, [^{111}In]**91** did not efficiently reach the brain of mice, and there was no specific increase in the brains of Tg mice compared with control mice, which indicated that [^{111}In]**91** could not penetrate the BBB and bind to Aβ plaques in the brain. Further micro-SPECT imaging studies confirmed that the radioactivity of [^{111}In]**91** was not found in either Tg or WT brains.

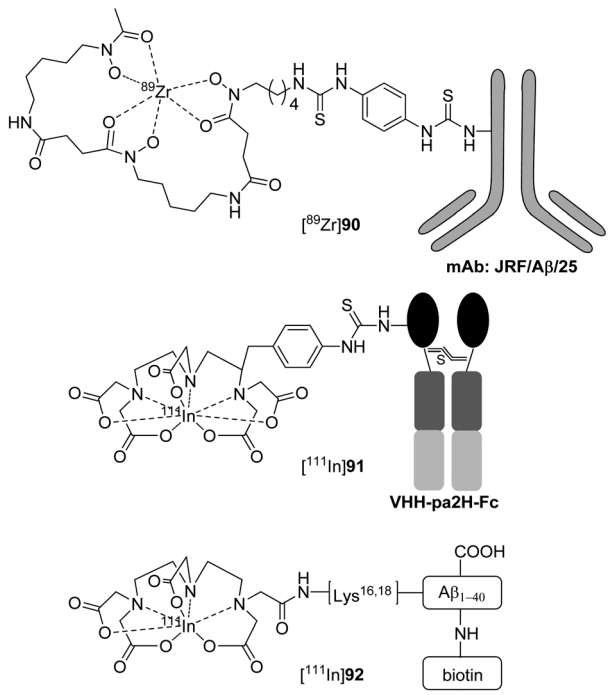

Fig. 14 Chemical structures of ^{89}Zr- and ^{111}In-labeled mAbs and Aβ peptides.

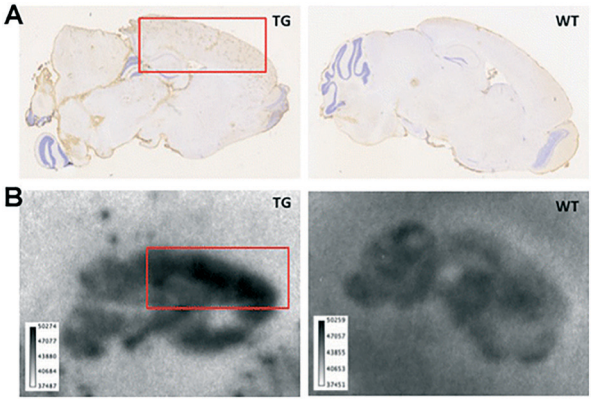

Fig. 15 Immunostaining (A) and *in vitro* autoradiography (B) on brain sections of 8 month-old APPPS1-21 Tg mice (left) and age-matched WT mice (right). Red squares indicate cortical regions with known high Aβ deposition. Adapted from ref. 82.

Compared with the classical immunohistochemical techniques for mAbs against Aβ, radiolabeled Aβ analogs enable more sensitive detection of Aβ plaques. Therefore, radiolabeled $Aβ_{1–42}$ and $Aβ_{1–40}$ analogs could be used for amyloid imaging in living patients with AD. Pardridge *et al.* reported an ^{111}In-labeled $Aβ_{1–40}$ analogue that contained biotin at the amino terminus and a DTPA chelator conjugated to one of the internal lysine residues ([^{111}In]**92**, [^{111}In]DTPA–[*N*-biotin]–$Aβ_{1–40}$, Fig. 14).[99] Film autoradiography studies showed that [^{111}In]**92** could intensely bind to the Aβ plaques in brain sections of patients with AD. However, quantitative binding studies and *in vivo* kinetic studies of [^{111}In]**92** were not reported.

3. Non-radioactive ruthenium and rhenium complexes binding to Aβ species

Owing to the strong spin–orbit coupling, heavy-metal complexes, which have highly intense phosphorescent emission with long lifetimes, are alternative choices to short-lived conventional organic fluorescent probes for the staining of different cellular compartments, monitoring of intracellular biological functions, and targeted bioimaging *in vivo*.[100] To date, heavy-metal complexes, including ruthenium and rhenium with d^6 electron configurations, have been evaluated as Aβ specific probes to monitor the formation of Aβ oligomers/fibrils or label Aβ deposits in tissue specimens.[28]

Murray *et al.* first investigated a cationic dye ruthenium red (ammoniated ruthenium oxychloride, **93**, Fig. 16) as an Aβ labeling agent.[101] Under light microscopy, Aβ plaques in brain sections of Tg2576 mice were dyed red by **93**; under cross-polarization, birefringence was observed when **93** bound to Aβ plaques. However, in addition to Aβ plaques, neurons in the dentate cellular layer of the hippocampus and the Purkinje layer of the cerebellum were also stained by **93**, which is undesirable for Aβ-specific dyes. The binding mechanism of **93** to Aβ fibrils was electrostatic interaction. This

 This journal is © The Royal Society of Chemistry 2017

Published on 16 May 2017. Downloaded by RSC Internal on 31/05/2018 13:36:39.

was confirmed because divalent cations, such as calcium, could displace **93** from its binding site in the Aβ plaques and remove the red coloration. In addition, upon binding to Aβ fibrils, **93** showed birefringence and induced circular dichroic bands at 540 nm owing to induced chirality. Overall, the chirality and cation binding mechanism of **93** to Aβ fibrils may be useful in the development of novel amyloid labeling methods, as well as novel AD imaging techniques.

Dipyridophenazine (DPPZ) ruthenium complexes demonstrated strong photoluminescence in the presence of Aβ fibril aggregates[102] or α-synuclein aggregates,[103] which made them ideal candidates for the monitoring and inhibition of the formation process of Aβ oligomers/fibrils. Based on these findings, Carlos *et al.* reported a novel ruthenium complex (**94**, Fig. 16) for multi-target treatment of AD.[104] Complex **94** displayed inhibitory activity on both human AChE and BuChE without appreciable cytotoxicity. More importantly, complex **94** displayed non-covalent interactions with Aβ, and the high sensitivity of **94** to Aβ enabled real-time observation of the conformational changes of Aβ monomers to protofibrils.

Unlike the direct interaction of the ruthenium complex with Aβ species, Rajagopal *et al.* reported a new ruthenium complex **95** (Fig. 16) intercalated with a RNA aptamer, which could selectively bind to the Aβ monomer and soluble oligomer.[105] Complex **95** displayed strong luminescence intensity in the presence of the RNA aptamer, which was apparently reduced upon the addition of Aβ monomers. Moreover, atomic force microscopy indicated that the aptamer–**95** complex displayed a strong inhibitory effect on the aggregation of the Aβ peptides. Overall, this novel aptamer–Ru complex system as an Aβ sensor may contribute to the rapid diagnosis and inhibition of Aβ aggregation in clinical applications.

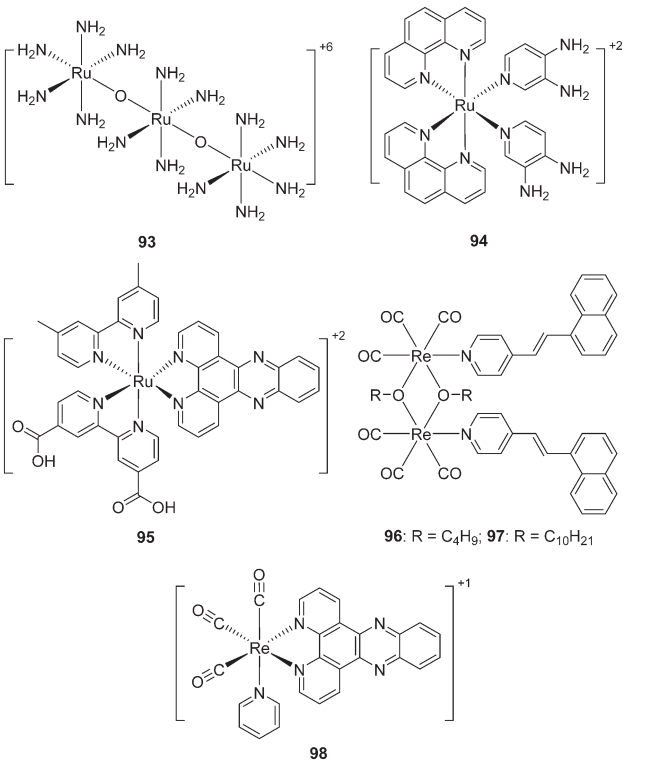

Fig. 16 Chemical structures of non-radioactive ruthenium and rhenium complexes.

Non-radioactive rhenium complexes can also be used as probes for the selective and sensitive detection of Aβ fibrils. Rajagopal *et al.* reported two alkoxy-bridged binuclear rhenium complexes (**96** and **97**, Fig. 16) with two stilbene-like 4-(1-naphthylvinyl)pyridines as Aβ binding motifs.[106] Luminescence titrations indicated that they exhibited strong fluorescence enhancement upon the addition of Aβ aggregates; the binding constants were calculated to be 2.2×10^5 and 2.0×10^5 M^{-1}, respectively. It is thought that the naphthalene moiety in these rhenium complexes might strongly interact with the hydrophobic regions of Aβ *via* π–π stacking interactions. This speculation was confirmed by docking studies between these rhenium complexes and the Aβ peptide.

Inspired by the previously observed increase of photoluminescence for ruthenium–DPPZ complexes with Aβ fibrils, Martí *et al.* investigated the photoluminescence properties of a rhenium complex ($[Re(CO)_3(dppz)(Py)]^+$, **98**, Fig. 16) upon interaction with fibrillar Aβ.[107] Upon binding to Aβ aggregates, **98** displayed an approximately 18-fold increase in photoluminescence in the primary light switching. Additionally, a significant time-dependent enhancement of photoluminescence was observed after light irradiation (secondary light switching). Under the optimized irradiation time (7200 s), a 105-fold increase in the photoluminescence was observed for **98** in the presence of Aβ fibrils. Unlike the ruthenium–DPPZ complexes, the two light-switching events observed for **98** were unprecedented, which may allow the monitoring of Aβ aggregation in real time and the addition of another dimension to the study of these rhenium complexes.

4. Non-radioactive gadolinium complexes for MRI

MRI offers noninvasive imaging of physiological structures and functions with remarkable spatial resolution. Compared with SPECT and PET, the MRI technique offers several advantages: does not require MRI radioactive probes and thus avoids exposure to radiation; possesses better resolution (50–200 μm) for research and clinical magnets; offers anatomical information for the quantification of amyloid deposits and the precise location of the deposition areas, which are critical for the evaluation of new treatments against AD at early stages; the lower cost and wide availability of MRI around the world.[108,109] However, the major limitation of MRI is its low sensitivity; MRI contrast in Aβ plaques is associated with iron accumulation, which leads to hypointense spots in T_2 and T_2^* or susceptibility-weighted images.[110,111] The detection of plaques that are weakly loaded with iron is more challenging. The best solution is to utilize exogenous contrast agents (CAs). So far, a modest number of MRI CAs for the diagnosis of AD have been developed, such as appropriate fluorinated small molecules,[112] Aβ-targeted iron oxide nanoparticles,[113]

Published on 16 May 2017. Downloaded by RSC Internal on 31/05/2018 13:36:39.

and conjugated gadolinium metal complexes.[114] Owing to their high paramagnetism, relaxation enhancement, favorable *in vivo* dynamics, and relatively high stability, gadolinium-based MRI CAs have shown great promise.[115] As the Aβ-targeted gadolinium complexes reported before 2016 are well documented in a review paper,[114] herein we include just two recently reported complexes.

Geraldes *et al.* reported a negatively charged Gd^{3+} complex (**99**, Fig. 17) with a neutral ethylenediamine linker between the DOTA and the Aβ-targeting PIB moieties.[116] In binding studies using a surface plasmon resonance method, **99** displayed a markedly reduced binding affinity for $A\beta_{1-40}$ aggregates (K_d = 194 ± 11 μM for La analogs), which is five orders of magnitude lower than that of PIB. More interestingly, TEM images and circular dichroism spectroscopy studies indicated that **99** appeared to inhibit the formation of $A\beta_{1-40}$ fibrils. Protein-based NMR also pointed to the interactions of paramagnetic **99** with $A\beta_{1-40}$ in the monomer state. However, further animal studies were not reported. Owing to its low Aβ affinity and expected low brain uptake, the authors proposed that complex **99** might not be adaptable for the early MRI detection of Aβ plaques in the brain of patients with AD, but could be helpful in animal studies with BBB opening and for *ex vivo* MRI.

By covalently coupling curcumin and gadolinium–DOTA into a natural drug delivery platform, poly(β-L-malic acid), Holler *et al.* reported a nanoimaging agent (NIA) **100** (Fig. 17).[117] The hydrodynamic diameter of **100** was 8.3 nm; each agent carried approximately 35 molecules of gadolinium–DOTA and curcumin. The detection of Aβ plaques by MRI in the presence of **100** displayed a significantly high contrast enhancement. Furthermore, a very clean staining pattern of Aβ plaques in mouse and human tissue, with a low background, was observed for **100**. These results revealed that the nanoimaging agent **100** had a good binding ability to Aβ plaques *in vitro*. After conjugation with the BBB penetrating agents, this NIA might be useful for the *in vivo* noninvasive diagnosis of AD.

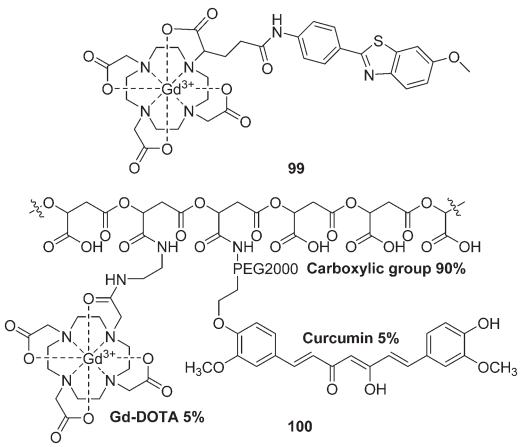

Fig. 17 Chemical structures of gadolinium complexes for MRI.

5. Conclusions

Although the etiology of AD and CAA is still not fully understood, Aβ deposition is considered to be one of the most important pathological features of these diseases. The development of Aβ-specific imaging probes for PET, SPECT, and MRI is of great importance in the early diagnosis and monitoring of the efficacy of anti-Aβ therapies for AD and CAA.

The past two decades have seen a remarkable increase in the development of ^{18}F- and ^{11}C-labeled Aβ probes for PET, some of which have been expanded into commercial applications. However, the development of ^{123}I- and ^{99m}Tc-labeled Aβ probes for SPECT is trailing far behind. At present, ^{99m}Tc is still the most appropriate radioisotope for SPECT imaging. In spite of continuous efforts to develop ^{99m}Tc-labeled probes with different ^{99m}Tc cores ($[^{99m}TcO]^{3+}$ and $[^{99m}Tc(CO)_3]^+$) and chelating agents (*e.g.*, MAMA, BAT, Ham, PAMA, IDA, and cyclopentadienyl tricarbonyl) for SPECT targeting of Aβ plaques inside the brain, none of the proposed probes could be used for the clinical diagnosis of AD. The main problem for these ^{99m}Tc-labeled probes is their low brain uptake: although they have sufficient affinity to Aβ plaques, they cannot penetrate the BBB and reach the target site. Thus, there is a need to further improve the brain uptake by structural modifications. As Aβ deposition was generated in the wall of cerebral vessels of CAA patients, there is no need to penetrate the entire BBB for imaging probes, which suggests a new application for the ^{99m}Tc-labeled probes with low brain uptake. Indeed, some probes have shown very promising results for CAA-specific imaging, as they can selectively label Aβ deposits in blood vessels, but not Aβ plaques, in the parenchyma of the brain. However, further experiments, especially human studies, will be required to confirm the utility of these ^{99m}Tc-labeled complexes as CAA imaging agents.

Other than ^{18}F, ^{11}C, and ^{99m}Tc, several radiometal nuclides such as ^{68}Ga, ^{64}Cu, ^{89}Zr, and ^{111}In have been incorporated into Aβ-specific small organic molecules, mAbs, and proteins *via* appropriate chelators (DOTA, DTPA, HBED, and DFO) as Aβ imaging agents for PET and SPECT. Similar to the ^{99m}Tc-labeled probes, they all displayed sufficient affinity for Aβ plaques, but poor BBB penetration owing to their large molecular weight and charged properties, which is unfavorable for the diagnosis of AD. However, through appropriate modifications, they may be used as imaging agents for CAA and diseases with peripheral amyloidosis.

Apart from the organic dyes, heavy-metal complexes, such as Ru and Re complexes, possessed interesting photophysical and photochemical characteristics. Some of the complexes displayed relatively long photoluminescence lifetimes and strong luminescence intensities when bound to Aβ species, which could be used as sensitive probes for the study of Aβ aggregation or labeling of Aβ deposits in tissue specimens. Compared with SPECT and PET, MRI offers an alternative approach for the detection of Aβ deposits in the brain. However, further efforts should be made to improve the Aβ binding affinity and the BBB penetrability of the reported gadolinium-based CAs.

 This journal is © The Royal Society of Chemistry 2017

Published on 16 May 2017. Downloaded by RSC Internal on 31/05/2018 13:36:39.

Conflict of interest

The authors declare no competing interests.

Acknowledgements

This work was funded by the National Natural Science Foundation of China (No. 21201019 and 21571022) and the National Science and Technology Major Projects for Major New Drugs Innovation and Development (No. 2014ZX09507007-002).

Notes and references

1 E. D. Roberson and L. Mucke, *Science*, 2006, **314**, 781.
2 E. E. Smith and S. M. Greenberg, *Stroke*, 2009, **40**, 2601–2606.
3 A. Viswanathan and S. M. Greenberg, *Ann. Neurol.*, 2011, **70**, 871–880.
4 W. D. Brenowitz, P. T. Nelson, L. M. Besser, K. B. Heller and W. A. Kukull, *Neurobiol. Aging*, 2015, **36**, 2702–2708.
5 J. A. Nicoll, M. Yamada, J. Frackowiak, B. Mazur-Kolecka and R. O. Weller, *Neurobiol. Aging*, 2004, **25**, 589–597 discussion 603-584.
6 K. A. Jellinger, *J. Neural Transm.*, 2002, **109**, 813–836.
7 J. Hardy, *J. Alzheimer's Dis.*, 2006, **9**, 151–153.
8 J. Hardy and D. J. Selkoe, *Science*, 2002, **297**, 353.
9 J. D. Fryer, K. Simmons, M. Parsadanian, K. R. Bales, S. M. Paul, P. M. Sullivan and D. M. Holtzman, *J. Neurosci.*, 2005, **25**, 2803–2810.
10 J. Attems, F. Lintner and K. A. Jellinger, *Acta Neuropathol.*, 2004, **107**, 283–291.
11 C. A. Mathis, Y. Wang and W. E. Klunk, *Curr. Pharm. Des.*, 2004, **10**, 1469–1492.
12 K. Herholz, *Lancet Neurol.*, 2012, **11**, 652–653.
13 C. C. Rowe and V. L. Villemagne, *J. Nucl. Med.*, 2011, **52**, 1733–1740.
14 M. Cui, *Curr. Med. Chem.*, 2014, **21**, 82–112.
15 A. Coimbra, D. S. Williams and E. D. Hostetler, *Curr. Top. Med. Chem.*, 2006, **6**, 629–647.
16 M. D. Ikonomovic, W. E. Klunk, E. E. Abrahamson, C. A. Mathis, J. C. Price, N. D. Tsopelas, B. J. Lopresti, S. Ziolko, W. Bi, W. R. Paljug, M. L. Debnath, C. E. Hope, B. A. Isanski, R. L. Hamilton and S. T. DeKosky, *Brain*, 2008, **131**, 1630–1645.
17 W. E. Klunk, H. Engler, A. Nordberg, Y. Wang, G. Blomqvist, D. P. Holt, M. Bergstrom, I. Savitcheva, G. F. Huang, S. Estrada, B. Ausen, M. L. Debnath, J. Barletta, J. C. Price, J. Sandell, B. J. Lopresti, A. Wall, P. Koivisto, G. Antoni, C. A. Mathis and B. Langstrom, *Ann. Neurol.*, 2004, **55**, 306–319.
18 C. A. Mathis, Y. Wang, D. P. Holt, G. F. Huang, M. L. Debnath and W. E. Klunk, *J. Med. Chem.*, 2003, **46**, 2740–2754.
19 K. Heurling, A. Leuzy, E. R. Zimmer, M. Lubberink and A. Nordberg, *Eur. J. Nucl. Med. Mol. Imaging*, 2016, **43**, 362–373.
20 M. Koole, D. M. Lewis, C. Buckley, N. Nelissen, M. Vandenbulcke, D. J. Brooks, R. Vandenberghe and K. Van Laere, *J. Nucl. Med.*, 2009, **50**, 818–822.
21 D. F. Wong, P. B. Rosenberg, Y. Zhou, A. Kumar, V. Raymont, H. T. Ravert, R. F. Dannals, A. Nandi, J. R. Brasic, W. Ye, J. Hilton, C. Lyketsos, H. F. Kung, A. D. Joshi, D. M. Skovronsky and M. J. Pontecorvo, *J. Nucl. Med.*, 2010, **51**, 913–920.
22 J. Lister-James, M. J. Pontecorvo, C. Clark, A. D. Joshi, M. A. Mintun, W. Zhang, N. Lim, Z. Zhuang, G. Golding, S. R. Choi, T. E. Benedum, P. Kennedy, F. Hefti, A. P. Carpenter, H. F. Kung and D. M. Skovronsky, *Semin. Nucl. Med.*, 2011, **41**, 300–304.
23 H. F. Kung, S. R. Choi, W. Qu, W. Zhang and D. Skovronsky, *J. Med. Chem.*, 2010, **53**, 933–941.
24 V. L. Villemagne, K. Ong, R. S. Mulligan, G. Holl, S. Pejoska, G. Jones, G. O'Keefe, U. Ackerman, H. Tochon-Danguy, J. G. Chan, C. B. Reininger, L. Fels, B. Putz, B. Rohde, C. L. Masters and C. C. Rowe, *J. Nucl. Med.*, 2011, **52**, 1210–1217.
25 C. C. Rowe, U. Ackerman, W. Browne, R. Mulligan, K. L. Pike, G. O'Keefe, H. Tochon-Danguy, G. Chan, S. U. Berlangieri, G. Jones, K. L. Dickinson-Rowe, H. P. Kung, W. Zhang, M. P. Kung, D. Skovronsky, T. Dyrks, G. Holl, S. Krause, M. Friebe, L. Lehman, S. Lindemann, L. M. Dinkelborg, C. L. Masters and V. L. Villemagne, *Lancet Neurol.*, 2008, **7**, 129–135.
26 Z. Zha, S. R. Choi, K. Ploessl, B. P. Lieberman, W. Qu, F. Hefti, M. Mintun, D. Skovronsky and H. F. Kung, *J. Med. Chem.*, 2011, **54**, 8085–8098.
27 B. H. Han, M. L. Zhou, A. K. Vellimana, E. Milner, D. H. Kim, J. K. Greenberg, W. Chu, R. H. Mach and G. J. Zipfel, *Mol. Neurodegener.*, 2011, **6**, 86.
28 D. J. Hayne, S. Lim and P. S. Donnelly, *Chem. Soc. Rev.*, 2014, **43**, 6701–6715.
29 S. S. Jurisson and J. D. Lydon, *Chem. Rev.*, 1999, **99**, 2205–2218.
30 J. L. Hickey and P. S. Donnelly, *Coord. Chem. Rev.*, 2012, **256**, 2367–2380.
31 S. Liu and D. S. Edwards, *Chem. Rev.*, 1999, **99**, 2235–2268.
32 G. Bandoli, F. Tisato, A. Dolmella and S. Agostini, *Coord. Chem. Rev.*, 2006, **250**, 561–573.
33 N. A. Dezutter, T. J. de Groot, R. H. Busson, G. A. Janssen and A. M. Verbruggen, *J. Labelled Compd. Radiopharm.*, 1999, **42**, 309–324.
34 N. A. Dezutter, R. J. Dom, T. J. de Groot, G. M. Bormans and A. M. Verbruggen, *Eur. J. Nucl. Med.*, 1999, **26**, 1392–1399.
35 K. Serdons, T. Verduyckt, J. Cleynhens, G. Bormans and A. Verbruggen, *J. Labelled Compd. Radiopharm.*, 2008, **51**, 357–367.
36 X. Chen, P. Yu, L. Zhang and B. Liu, *Bioorg. Med. Chem. Lett.*, 2008, **18**, 1442–1445.
37 K. Serdons, T. Verduyckt, J. Cleynhens, C. Terwinghe, L. Mortelmans, G. Bormans and A. Verbruggen, *Bioorg. Med. Chem. Lett.*, 2007, **17**, 6086–6090.
38 X. Wang, M. Cui, P. Yu, Z. Li, Y. Yang, H. Jia and B. Liu, *Bioorg. Med. Chem. Lett.*, 2012, **22**, 4327–4331.
39 Y. Cheng, M. Ono, H. Kimura, M. Ueda and H. Saji, *J. Med. Chem.*, 2012, **55**, 2279–2286.
40 M. Ono, Y. Fuchi, T. Fuchigami, N. Kobashi, H. Kimura, M. Haratake, H. Saji and M. Nakayama, *ACS Med. Chem. Lett.*, 2010, **1**, 443–447.

Published on 16 May 2017. Downloaded by RSC Internal on 31/05/2018 13:36:39.

41 M. Ono, R. Ikeoka, H. Watanabe, H. Kimura, T. Fuchigami, M. Haratake, H. Saji and M. Nakayama, *Bioorg. Med. Chem. Lett.*, 2010, **20**, 5743–5748.
42 M. Ono, R. Ikeoka, H. Watanabe, H. Kimura, T. Fuchigami, M. Haratake, H. Saji and M. Nakayama, *ACS Chem. Neurosci.*, 2010, **1**, 598–607.
43 M. Sagnou, D. Benaki, C. Triantis, T. Tsotakos, V. Psycharis, C. P. Raptopoulou, I. Pirmettis, M. Papadopoulos and M. Pelecanou, *Inorg. Chem.*, 2011, **50**, 1295–1303.
44 M. Cui, R. Tang, Z. Li, H. Ren and B. Liu, *Bioorg. Med. Chem. Lett.*, 2011, **21**, 1064–1068.
45 Y. Yang, M. Cui, B. Jin, X. Wang, Z. Li, P. Yu, J. Jia, H. Fu, H. Jia and B. Liu, *Eur. J. Med. Chem.*, 2013, **64**, 90–98.
46 J. Zhang, X. Zhou and X. Qin, *J. Radioanal. Nucl. Chem.*, 2012, **292**, 1377–1383.
47 X. Wang, M. Cui, J. Jia and B. Liu, *Eur. J. Med. Chem.*, 2015, **89**, 331–339.
48 X. Zhang, P. Yu, Y. Yang, Y. Hou, C. Peng, Z. Liang, J. Lu, B. Chen, J. Dai, B. Liu and M. Cui, *Bioconjugate Chem.*, 2016, **27**, 2493–2504.
49 K. Thipyapong, T. Uehara, Y. Tooyama, H. Braband, R. Alberto and Y. Arano, *Inorg. Chem.*, 2011, **50**, 992–998.
50 M. Nakayama, L. C. Xu, Y. Koga, K. Harada, A. Sugii, H. Nakayama, S. Tomiguchi, A. Kojima, Y. Ohyama, M. Takahashi and I. Okabayashi, *Appl. Radiat. Isot.*, 1997, **48**, 571–577.
51 M. Nakayama, H. Saigo, A. Koda, K. Ozeki, K. Harada, A. Sugii, S. Tomiguchi, A. Kojima, M. Hara, R. Nakashima, Y. Ohyama, M. Takahashi, J. Takata and Y. Karube, *Appl. Radiat. Isot.*, 1994, **45**, 735–740.
52 S. Iikuni, M. Ono, H. Watanabe, K. Matsumura, M. Yoshimura, N. Harada, H. Kimura, M. Nakayama and H. Saji, *Mol. Pharmaceutics*, 2014, **11**, 1132–1139.
53 S. Iikuni, M. Ono, H. Watanabe, K. Matsumura, M. Yoshimura, H. Kimura, H. Ishibashi-Ueda, Y. Okamoto, M. Ihara and H. Saji, *Sci. Rep.*, 2016, **6**, 25990.
54 S. Iikuni, M. Ono, H. Watanabe, M. Yoshimura, H. Ishibashi-Ueda, M. Ihara and H. Saji, *PLoS One*, 2016, **11**, e0163969.
55 D. J. Hayne, J. M. White, C. A. McLean, V. L. Villemagne, K. J. Barnham and P. S. Donnelly, *Inorg. Chem.*, 2016, **55**, 7944–7953.
56 M. Morais, A. Paulo, L. Gano, I. Santos and J. D. G. Correia, *J. Organomet. Chem.*, 2013, **744**, 125–139.
57 R. Alberto, R. Schibli, R. Waibel, U. Abram and A. P. Schubiger, *Coord. Chem. Rev.*, 1999, **190–192**, 901–919.
58 R. Alberto, K. Ortner, N. Wheatley, R. Schibli and A. P. Schubiger, *J. Am. Chem. Soc.*, 2001, **123**, 3135–3136.
59 R. Schibli, R. La Bella, R. Alberto, E. Garcia-Garayoa, K. Ortner, U. Abram and P. A. Schubiger, *Bioconjugate Chem.*, 2000, **11**, 345–351.
60 D. Satpati, A. Korde, H. D. Sarma and S. Banerjee, *J. Radioanal. Nucl. Chem.*, 2014, **302**, 1339–1344.
61 D. J. Hayne, A. J. North, M. Fodero-Tavoletti, J. M. White, L. W. Hung, A. Rigopoulos, C. A. McLean, P. A. Adlard, U. Ackermann, H. Tochon-Danguy, V. L. Villemagne, K. J. Barnham and P. S. Donnelly, *Dalton Trans.*, 2015, **44**, 4933–4944.
62 J. Jia, M. Cui, J. Dai, X. Wang, Y.-S. Ding, H. Jia and B. Liu, *MedChemComm*, 2014, **5**, 153–158.
63 J. Jia, M. Cui, J. Dai and B. Liu, *Mol. Pharmaceutics*, 2015, **12**, 2937–2946.
64 J. Jia, M. Cui, J. Dai and B. Liu, *Dalton Trans.*, 2015, **44**, 6406–6415.
65 J. Jia, K. Zhou, J. Dai, B. Liu and M. Cui, *Eur. J. Med. Chem.*, 2016, **124**, 763–772.
66 J. Bernard, K. Ortner, B. Spingler, H. J. Pietzsch and R. Alberto, *Inorg. Chem.*, 2003, **42**, 1014–1022.
67 C. Y. Chan, A. Noor, C. A. McLean, P. S. Donnelly and P. J. Barnard, *Chem. Commun.*, 2017, **53**, 2311–2314.
68 I. Velikyan, *Theranostics*, 2014, **4**, 47–80.
69 F. Roesch and P. J. Riss, *Curr. Top. Med. Chem.*, 2010, **10**, 1633–1668.
70 M. Fani, J. P. André and H. R. Maecke, *Contrast Media Mol. Imaging*, 2008, **3**, 53–63.
71 D. Cressier, M. Dhilly, T. T. Cao Pham, F. Fillesoye, F. Gourand, A. Maïza, A. F. Martins, J.-F. Morfin, C. F. G. C. Geraldes, É. Tóth and L. Barré, *Mol. Imaging Biol.*, 2016, **18**, 334–343.
72 H. Watanabe, M. Ono, S. Iikuni, M. Yoshimura, K. Matsumura, H. Kimura and H. Saji, *Bioorg. Med. Chem. Lett.*, 2014, **24**, 4834–4837.
73 M. Eder, B. Wangler, S. Knackmuss, F. LeGall, M. Little, U. Haberkorn, W. Mier and M. Eisenhut, *Eur. J. Nucl. Med. Mol. Imaging*, 2008, **35**, 1878–1886.
74 R. J. Motekaitis, A. E. Martell and M. J. Welch, *Inorg. Chem.*, 1990, **29**, 1463–1467.
75 K. Chauhan, A. Datta, A. Adhikari, K. Chuttani, A. Kumar Singh and A. K. Mishra, *Org. Biomol. Chem.*, 2014, **12**, 7328–7337.
76 Z. Zha, J. Song, S. R. Choi, Z. Wu, K. Ploessl, M. Smith and H. Kung, *Bioconjugate Chem.*, 2016, **27**, 1314–1323.
77 M. Cui, M. Ono, H. Kimura, B. Liu and H. Saji, *J. Med. Chem.*, 2011, **54**, 2225–2240.
78 J. Rokka, A. Snellman, C. Zona, B. La Ferla, F. Nicotra, M. Salmona, G. Forloni, M. Haaparanta-Solin, J. O. Rinne and O. Solin, *Bioorg. Med. Chem.*, 2014, **22**, 2753–2762.
79 E. K. Ryu, Y. S. Choe, K. H. Lee, Y. Choi and B. T. Kim, *J. Med. Chem.*, 2006, **49**, 6111–6119.
80 M. Asti, E. Ferrari, S. Croci, G. Atti, S. Rubagotti, M. Iori, P. C. Capponi, A. Zerbini, M. Saladini and A. Versari, *Inorg. Chem.*, 2014, **53**, 4922–4933.
81 H. Watanabe, A. Kawasaki, K. Sano, M. Ono and H. Saji, *Bioorg. Med. Chem.*, 2016, **24**, 3618–3623.
82 J. Fissers, A. M. Waldron, T. De Vijlder, B. Van Broeck, D. J. Pemberton, M. Mercken, P. Van Der Veken, J. Joossens, K. Augustyns, S. Dedeurwaerdere, S. Stroobants, S. Staelens and L. Wyffels, *Mol. Imaging Biol.*, 2016, **18**, 598–605.
83 J. L. Lange, D. J. Hayne, P. Roselt, C. A. McLean, J. M. White and P. S. Donnelly, *J. Inorg. Biochem.*, 2016, **162**, 274–279.
84 P. J. Blower, J. S. Lewis and J. Zweit, *Nucl. Med. Biol.*, 1996, **23**, 957–980.

 This journal is © The Royal Society of Chemistry 2017

Published on 16 May 2017. Downloaded by RSC Internal on 31/05/2018 13:36:39.

85 S. V. Smith, *J. Inorg. Biochem.*, 2004, **98**, 1874–1901.
86 A. Nordberg, *Lancet Neurol.*, 2004, **3**, 519–527.
87 D. McLean, M. J. Cooke, R. Albay 3rd, C. Glabe and M. S. Shoichet, *ACS Chem. Neurosci.*, 2013, **4**, 613–623.
88 C. G. Glabe, *Trends Biochem. Sci.*, 2004, **29**, 542–547.
89 D. Sehlin, X. T. Fang, L. Cato, G. Antoni, L. Lannfelt and S. Syvanen, *Nat. Commun.*, 2016, **7**, 10759.
90 K. Magnusson, D. Sehlin, S. Syvanen, M. M. Svedberg, O. Philipson, L. Soderberg, K. Tegerstedt, M. Holmquist, P. Gellerfors, V. Tolmachev, G. Antoni, L. Lannfelt, H. Hall and L. N. Nilsson, *J. Alzheimer's Dis.*, 2013, **37**, 29–40.
91 D. McLean, M. J. Cooke, Y. Wang, D. Green, P. E. Fraser, P. S. George-Hyslop and M. S. Shoichet, *PLoS One*, 2012, **7**, e51958.
92 G. Fischer, U. Seibold, R. Schirrmacher, B. Wängler and C. Wängler, *Molecules*, 2013, **18**, 6469–6490.
93 G. W. Severin, J. W. Engle, R. J. Nickles and T. E. Barnhart, *Med. Chem.*, 2011, **7**, 389–394.
94 L. R. Perk, M. J. Vosjan, G. W. Visser, M. Budde, P. Jurek, G. E. Kiefer and G. A. van Dongen, *Eur. J. Nucl. Med. Mol. Imaging*, 2010, **37**, 250–259.
95 M. J. Vosjan, L. R. Perk, G. W. Visser, M. Budde, P. Jurek, G. E. Kiefer and G. A. van Dongen, *Nat. Protoc.*, 2010, **5**, 739–743.
96 M. J. Miller, *Chem. Rev.*, 1989, **89**, 1563–1579.
97 S. Chakraborty and S. Liu, *Curr. Top. Med. Chem.*, 2010, **10**, 1113–1134.
98 M. Rotman, M. M. Welling, M. L. van den Boogaard, L. G. Moursel, L. M. van der Graaf, M. A. van Buchem, S. M. van der Maarel and L. van der Weerd, *Nucl. Med. Biol.*, 2015, **42**, 695–702.
99 A. Kurihara and W. M. Pardridge, *Bioconjugate Chem.*, 2000, **11**, 380–386.
100 A. E. Friedman, J. C. Chambron, J. P. Sauvage, N. J. Turro and J. K. Barton, *J. Am. Chem. Soc.*, 1990, **112**, 4960–4962.
101 N. P. Cook, C. M. Archer, J. N. Fawver, H. E. Schall, J. Rodriguez-Rivera, K. T. Dineley, A. A. Martí and I. V. J. Murray, *ACS Chem. Neurosci.*, 2013, **4**, 379–384.
102 N. P. Cook, V. Torres, D. Jain and A. A. Martí, *J. Am. Chem. Soc.*, 2011, **133**, 11121–11123.
103 N. P. Cook, K. Kilpatrick, L. Segatori and A. A. Martí, *J. Am. Chem. Soc.*, 2012, **134**, 20776–20782.
104 D. E. S. Silva, M. P. Cali, W. M. Pazin, E. Carlos-Lima, M. T. Salles Trevisan, T. Venâncio, M. Arcisio-Miranda, A. S. Ito and R. M. Carlos, *J. Med. Chem.*, 2016, **59**, 9215–9227.
105 E. Babu, P. Muthu Mareeswaran, V. Sathish, S. Singaravadivel and S. Rajagopal, *Talanta*, 2015, **134**, 348–353.
106 V. Sathish, E. Babu, A. Ramdass, Z.-Z. Lu, M. Velayudham, P. Thanasekaran, K.-L. Lu and S. Rajagopal, *Talanta*, 2014, **130**, 274–279.
107 A. Aliyan, B. Kirby, C. Pennington and A. A. Martí, *J. Am. Chem. Soc.*, 2016, **138**, 8686–8689.
108 Y. Z. Wadghiri, D. M. Hoang, T. Wisniewski and E. M. Sigurdsson, *Methods Mol. Biol.*, 2012, **849**, 435–451.
109 D. E. Huddleston and S. A. Small, *Nat. Clin. Pract. Neurol.*, 2005, **1**, 96–105.
110 C. R. Jack Jr., M. Garwood, T. M. Wengenack, B. Borowski, G. L. Curran, J. Lin, G. Adriany, O. H. Grohn, R. Grimm and J. F. Poduslo, *Magn. Reson. Med.*, 2004, **52**, 1263–1271.
111 M. Rohrer, H. Bauer, J. Mintorovitch, M. Requardt and H. J. Weinmann, *Invest. Radiol.*, 2005, **40**, 715–724.
112 I. Tooyama, D. Yanagisawa, H. Taguchi, T. Kato, K. Hirao, N. Shirai, T. Sogabe, N. F. Ibrahim, T. Inubushi and S. Morikawa, *Ageing Res. Rev.*, 2016, **30**, 85–94.
113 N. Beckmann, C. Gerard, D. Abramowski, C. Cannet and M. Staufenbiel, *J. Neurosci.*, 2011, **31**, 1023–1031.
114 M. Salerno and D. Santo Domingo Porqueras, *Coord. Chem. Rev.*, 2016, **327–328**, 27–34.
115 P. Verwilst, S. Park, B. Yoon and J. S. Kim, *Chem. Soc. Rev.*, 2015, **44**, 1791–1806.
116 A. F. Martins, A. C. Oliveira, J.-F. Morfin, D. V. Laurents, É. Tóth and C. F. G. C. Geraldes, *J. Biol. Inorg. Chem.*, 2016, **21**, 83–99.
117 R. Patil, P. R. Gangalum, S. Wagner, J. Portilla-Arias, H. Ding, A. Rekechenetskiy, B. Konda, S. Inoue, K. L. Black, J. Y. Ljubimova and E. Holler, *Macromol. Biosci.*, 2015, **15**, 1212–1217.